Appendix A

Characterization of Magneto-Optical Media

Roger A. Hajjar , *Te-ho Wu* and M. Mansuripur
Optical Sciences Center
University of Arizona
Tucson, AZ 85721

Amorphous rare earth-transition metal (RE-TM) alloys and compositionally modulated *TM TM* films (prepared in the laboratories of the ODSC sponsors) are characterized in terms of their magnetic, magneto-optic and galvanomagnetic properties. The loop tracer, vibrating sample magnetometer (VSM), and the Rutherford Backscattering facility (RBS) have been used to characterize and analyze the various properties of these magneto-optical storage media.

The loop tracer consists of a 21 kGauss electromagnet (4" diameter pole piece, 2" gap). The magnet has a rotating stage that allows its field to be applied both perpendicular to and in the plane of the sample. Samples of up to 1" in diameter can be analyzed in a cryogenic dewar cycling temperatures from 80 K to 475 K. The DC differential detection technique is used to measure the magneto-optical Kerr effect at the 633 nm HeNe wavelength. Ellipticity can also be measured with the insertion of a quarter-wave-plate. The magnetic properties such as coercivity and anisotropy constants at various temperatures are determined form the perpendicular and in-plane measurements of the polar Kerr effect[1] (KE). Galvanomagnetic and transport properties such as the Hall effect (HE), magnetoresistance (MR) and resistivity are measured with two mutually orthogonal pairs of point contacts at the sample surface[2].

a) Co/Pt Films : The *Co/Pt* films were prepared by Dr. *C*-J. Lin of IBM Almaden Research Center. These are multilayered films consisting of alternating ultrathin *Co* and *Pt* layers. The films were deposited by *e*-beam evaporation from *Co* and *Pt* sources onto glass substrates[3]. The periodicity and crystallographic structures were obtained by *X*-ray diffraction analyses and the composition was measured by both XRF and RBS. The total thickness of these films was nominally set to 30 nm where the thickness of the *Pt* layer was set to about 1.0 nm and the thickness of the *Co* layer varied from 0.2nm to 0.4 nm.

All samples show perpendicular magnetic anisotropy and rectangular hysteresis loop in perpendicular magnetic fields. Figures 1 through 4 show the various chracteristics of these films versus *Co* thickness. The remanent Kerr angle and Hall resistivity at room temperature are displayed in Fig. 1. Figure 2 shows the saturation magnetization M_s obtained from the VSM hysteresis loops and $\Delta\rho/\rho$ longitudinal obtained from the MR measurement when the field is in the plane of the sample. The value of $\Delta\rho/\rho$ is obtained from the peak of the longitudinal MR curve as shown in

Fig. 5. The linear trend of θ_k, ρ_H, M_s and $\Delta\rho/\rho$ (longitudinal peak) correlate with the increase of *Co* content in these films. From the magnetization data we find that the effective *Co* moment is around 1750 emu/cc which is considerably enhanced relative to that of bulk cobalt. This enhancement is believed to be due to the stretching of the cobalt lattice which makes it more atomic like (atomic spin polarization of *Co* is about twice as large as that of bulk *Co*)[4]. There is little evidence that *Pt* is polarized as far as we can tell from the *Ms* data. Evidently, more data points are needed in order to give a quantitative assesment of the *Pt* polarization.

Figure 3 displays the nucleation coercivity (H_c) and anisotropy field (H_k) for these films. Both H_c and H_k can be determined from four different measurements, namely : Kerr, Hall, VSM and MR measurements with the applied field being either perpendicular to or in the plane of the sample. The nucleation coercivity can be obtained from KE, HE or VSM hysteresis loops. We can also obtain *Hc* from the perpendicular MR measurement as illustrated in Figs. 7 and 8. The linear part of the curve in Fig. 8 has a negative slope of 3.1×10^{-8} per Oersted, which has its origin in the *s-d* scattering phenomenon as interpreted by Mott[5]. The peaks centered around the coercive field are caused by the scattering of the conduction electrons from the magnetization within the domain walls. These walls cause the resistivity to increase provided that their magnetic moments, while in the plane of the film, are also parallel to the direction of the current. Thus the height of the peaks in Fig. 8 is a measure of the volume fraction covered by the domain walls, while the width of the peaks corresponds to the transition region observed in the vicinity of H_c in the hysteresis loop.

The anisotropy field is determined from the initial part of the KE or HE in-plane measurement[1] (Fig. 6). Also, H_k can be roughly determined from the perpendicular and in-plane VSM measurement by extrapolating the intercept of the in-plane measurement with the saturation part of the hysteresis loop as shown in Fig. 9. H_k is also obtained from the longitudinal MR measurement as shown in Fig. 5. In this measurement, the sample is first saturated along the easy axis. The initial increase of resistivity with the applied field is due to the alignment of magnetization with the field. The maximum of $\Delta\rho/\rho$ (longitudinal) is reached at $H = H_k$. Once the magnetization and the field have been aligned, further increases in H cause a linear decrease of $\Delta\rho/\rho$ which, as mentioned before, is related to the *s-d* scattering. As shown in Fig. 3, the anisotropy field decreases with increasing cobalt layer thickness. As expected, H_k decreases from a positive value towards negative values, corresponding to an in-plane easy axis of magnetization for thick cobalt layers. A rough extrapolation shows that the crossing point between the perpendicular and in plane anisotropy regimes lies at about 0.7 nm of Co. For ultrathin *Co* (< 0.25 nm), the anisotropy field is reduced mainly due to the island-like formation of the *Co* layers that become discontinuous.

Figure 4 shows the magnitude of the slope due to *s-d* scattering obtained from the perpendicular MR measurement (see Fig. 8). The data obtained correlate to a certain extent with the total thickness of one period over the thickness of cobalt, $(t_{Co} + t_{Pt})/t_{Co}$. Note that for pure cobalt, where this ratio is equal to 1, the slope obtained is 3×10^{-8} per Oersted.

We have also measured the electrical resistivity using the Van der Pauw technique[6]. The resistivity reflects the character of the interfaces in superlattices. For reference, the resistivity of a thick (sputtered) cobalt sample (175 nm-thick) was found to be 14 $\mu\Omega.cm$, and those of pure *Pd* and *Pt* films (sputtered) were around 17 $\mu\Omega.cm$. The typical room temperature resistivity for a multilayer film is in the range of 30 - 60 $\mu\Omega.cm$. From this behaviour, we can assume that multilayers with abrupt interfaces should have a resistivity intermediate to those of the constituent metals while mixed interfaces will have resistivities as much as a factor of 10 higher. For the samples studied here, the *Co/Pt* films (30 nm-thick) have a typical resistivity of 45 $\mu\Omega.cm$, while similar *Co/Pd* samples (see next paragraph) have a resistivity of 37 $\mu\Omega.cm$. Adopting the above argument, we attribute the larger resistivity of the *Co/Pt* films to interfacial mixing between platinum and cobalt layers, and conclude that *Co/Pd* films have sharper interfaces.

b) Co/Pd Films : A series of Co/Pd multilayer films were fabricated by Dr. Charles Brucker of Kodak Research Laboratories. These are sputtered *Co* (0.2 nm)/*Pd* (.9 nm) films with thicknesses ranging from 5.5 nm to 87.5 nm. Figures 10 - 13 display the thickness-dependence of the magnetic, magneto-optic, and galvanomagnetic properties of these samples at room temperature. The Kerr rotation angle Θ_k measured from the film side is remarkably enhanced around 11 nm of thickness. This enhancement is due to optical interference between the rays reflected from the film surface and those reflected at the interface between film and substrate; the enhancement is *not* related to the multilayer structure of the film. Even though the concept of Kerr effect enhancement due to optical interference is well known, we revisit this topic for the sake of completeness.

Consider a magneto-optic film sandwiched between two mediums of indices n_1 and n_3. The MO layer has two indices of refraction denoted by n_2^+ and n_2^-, corresponding to left and right circularly polarized light. Knowing that linearly polarized light may be decomposed into left and right circular polarization, we write the Fresnel coefficients as :

$$r_1^{(\pm)} = \frac{n_2^{(\pm)} - n_1}{n_2^{(\pm)} + n_1}$$

for reflection off the top surface of the MO layer and :

$$r_2^{(\pm)} = \frac{n_3 - n_2^{(\pm)}}{n_3 + n_2^{(\pm)}}$$

for the reflection off the bottom surface of the MO layer. Assuming multiple reflections within the MO layer, we obtain a general expression of the total reflectivity as follows :

$$r^{(\pm)} = \frac{r_1^{(\pm)} + r_2^{(\pm)} \exp(-i\delta^{(\pm)})}{1 + r_1^{(\pm)} r_2^{(\pm)} \exp(-i\delta^{(\pm)})}$$

where $\delta^{(\pm)} = 4\pi\, n_2^{(\pm)} \times thickness/\lambda$. Calculation of Kerr rotation angle and ellipticity from the above equation is straightforward[7]. Figure 14 shows a calculated curve of Θ_k and ϵ_k versus film thickness. The magneto-optic refractive indices (at λ = 790 nm) are obtained from the literature for the film structure *Co*(0.2nm)/*Pd*(0.9nm) with a total thickness of 50 nm.

The electrical resistivity is displayed in Fig. 12 and shows a rapid increase for thicknesses below 16.5 nm. This increase in resistivity can be explained by the change in the film morphology, namely the film growth from an island structure to a continuous structure[8]. The change in the film morphology can also be observed in the magnetic properties such as the anisotropy, coercivity and saturation magnetization where a sharp decrease is observed below 16.5 nm (see Figs. 11 and 13). Note that, as expected, the Hall resistivity in Fig. 10 is independent of the magneto-optical interference effects discussed above and is closely related to the resistivity data. It can be shown[9] that $\rho_h \propto \gamma\rho^2$, where the coefficient γ is related to the spin-orbit coupling and goes to zero in the absence of spin-orbit coupling. Good agreement is obtained by fitting the data with the theory.

The *s-d* slope observed in these films is significantly larger than in *Co/Pt* films of approximately the same structure as shown in Figs. 15 and 16. This might be attributed to three different phenomena : The *d*-band structure of cobalt is becoming steeper and closer to the Fermi level (see reference 4), the induced magnetic polarization of *Pd*, or the extreme proximity of the *Pd* Fermi level to the edge of the *d*-band.

c) TbFeCo Films : A study of the thermomagnetic properties of TbFeCo films is currently underway. These are films of variable *Tb* content (ranging from 22.5% to 28%), and were prepared at the IBM Almaden Research Center. The films are deposited onto quartz substrates and consist of a quadrilayer structure of AlCr with an MO layer sandwiched between two dielectric SiN layers.

Figure 17 displays the saturation magnetization M_s versus temperature for these films. Figure 18 shows the T_{comp} and M_s as a function of *Tb* content. The sum of the anisotropy energy constants K_1 and K_2 at room temperature is displayed in Fig. 19. These parameters are obtained from the in-plane Kerr measurement[1]. The apparent reduction of K_u (i.e., $K_1 + K_2$) at the compensation point is not real, but is due to the fact that the maximum field strength in our experiment ($\simeq$ 21 KOe) is insufficient to tilt the magnetization away from the perpendicular direction.

Figure 20 shows a typical set of perpendicular and in-plane Kerr effect measurement results for the TbFeCo samples. The bottom frame in Fig. 20 shows the fitting of the normalized in-plane data to the theoretical model (normalization is by the height of the hysteresis loop); it is from this kind of fitting that the anisotropy constants K_1 and K_2 are determined.

Plots of the remanent Kerr angle and coercivity, obtained from the hysteresis loops, are shown in Fig. 21. We are currently measuring the temperature-dependence of the various properties of these films in order to determine their anisotropy constants as function of temperature.

REFERENCES

1 R.A. Hajjar, F.L. Zhou and M. Mansuripur, J.Appl. Phys. **67**, 5328 (1990).

2 R.A. Hajjar, M. Mansuripur and *H*-P.D. Shieh, to appear in J. Appl. Phys. (1991).

R.A. Hajjar, M. Mansuripur and *H*-P.D. Shieh, presented at MMM'90, to appear in J. Appl. Phys., April 1991.

3 C.-J. Lin and H.V. Do, IEEE MAG **26**, 1700 (1990).

4 R. H. Victora and J.M. Maclaren, "Calculated Magnetic and Electronic Properties of *Co/Pd* Superlattices", (unpublished Report).

5 N. F. Mott, Proc. Roy. Soc. A, (London) **153**, 699 (1936) and **56**, 368 (1936).

6 L. J. Van der Pauw, Philips Rev. **20**, 220 (1958).

7 M. Born and E. Wolf, "Principles of Optics", 6th edition, Pergamon Press.

8 S. Hachimoto,Y. Ochiai and K. Aso, J. Appl. Phys. **67**, 4429 (1990).

9 R. Karplus and J.M. Luttinger, Phys. Rev. **95**, 1154 (1954).

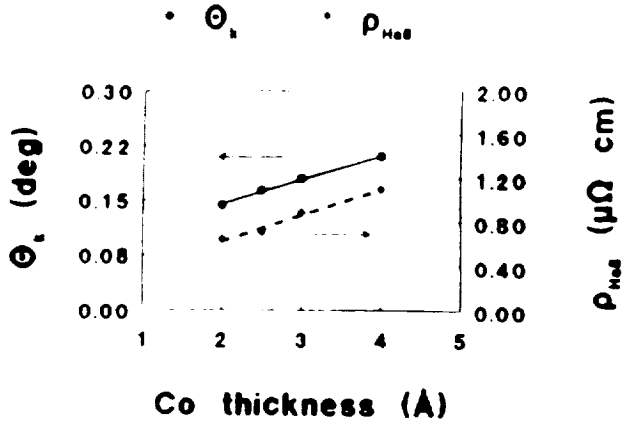

Fig. 1

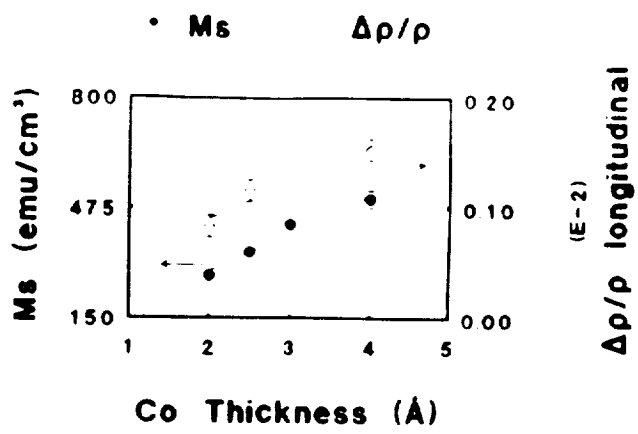

Fig. 2

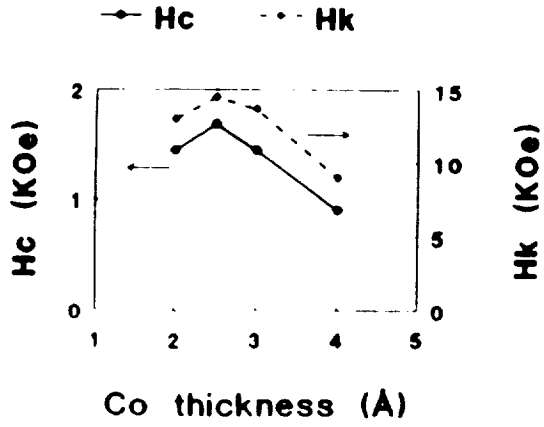

Fig. 3

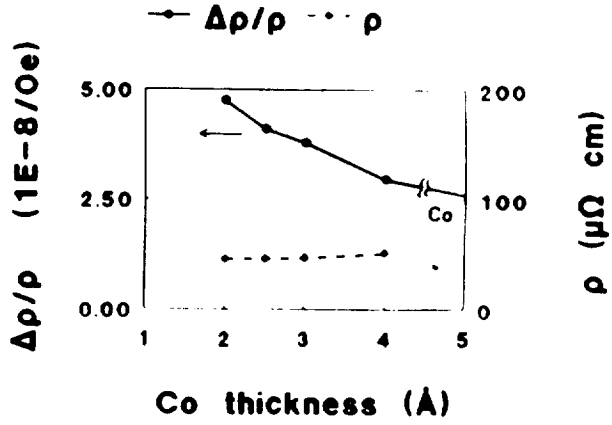

Fig. 4

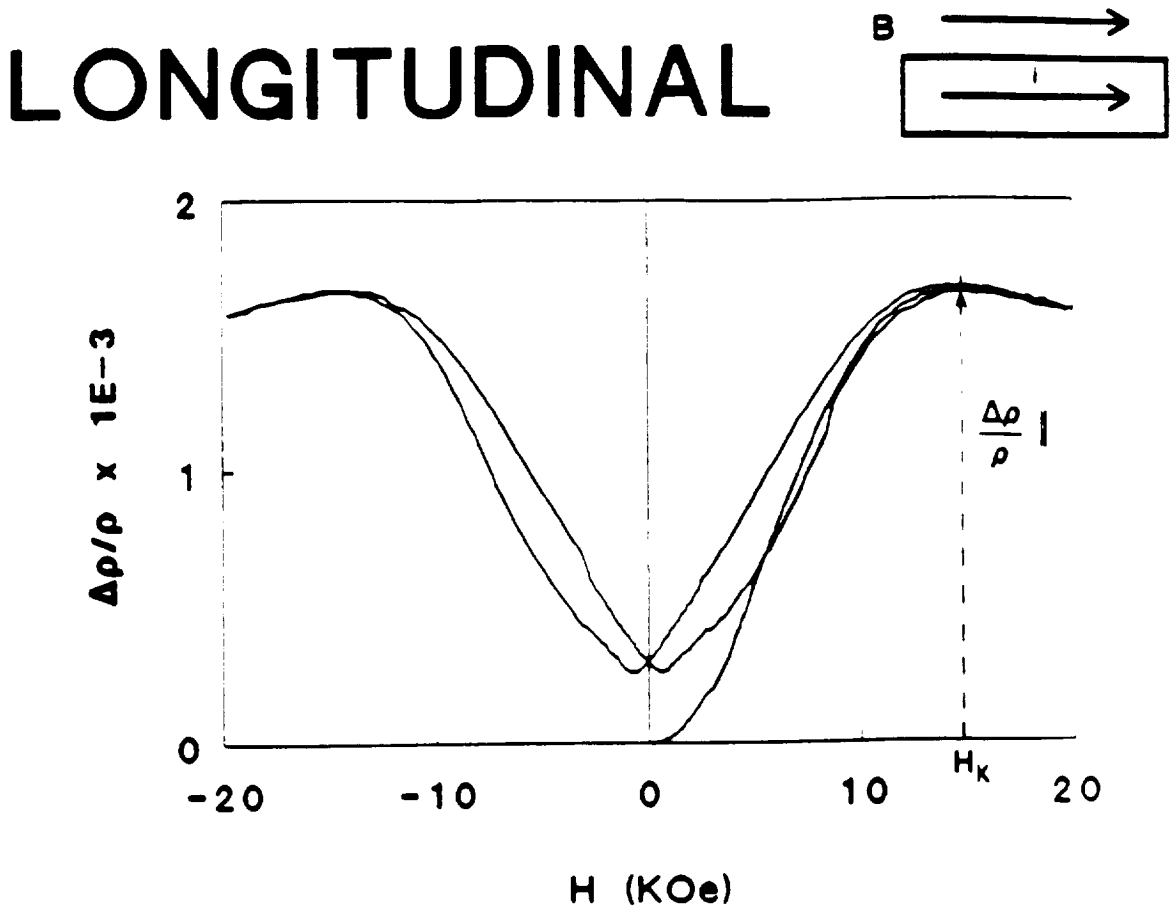
LONGITUDINAL
B
I
2
1
0
Δρ/ρ x 1E-3
Δρ/ρ
-20
-10
0
10
20
H_K
H (KOe)

Fig. 5

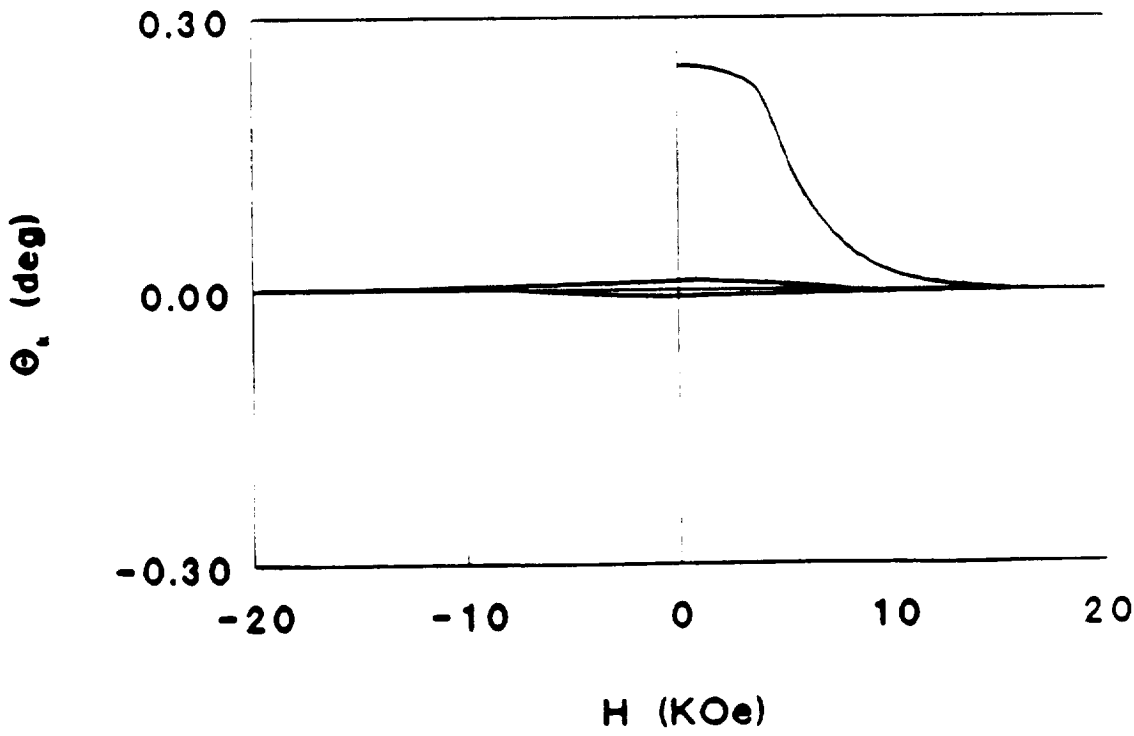
0.30
0.00
-0.30
Θ_k (deg)
-20
-10
0
10
20
H (KOe)

Fig. 6

Appendix A

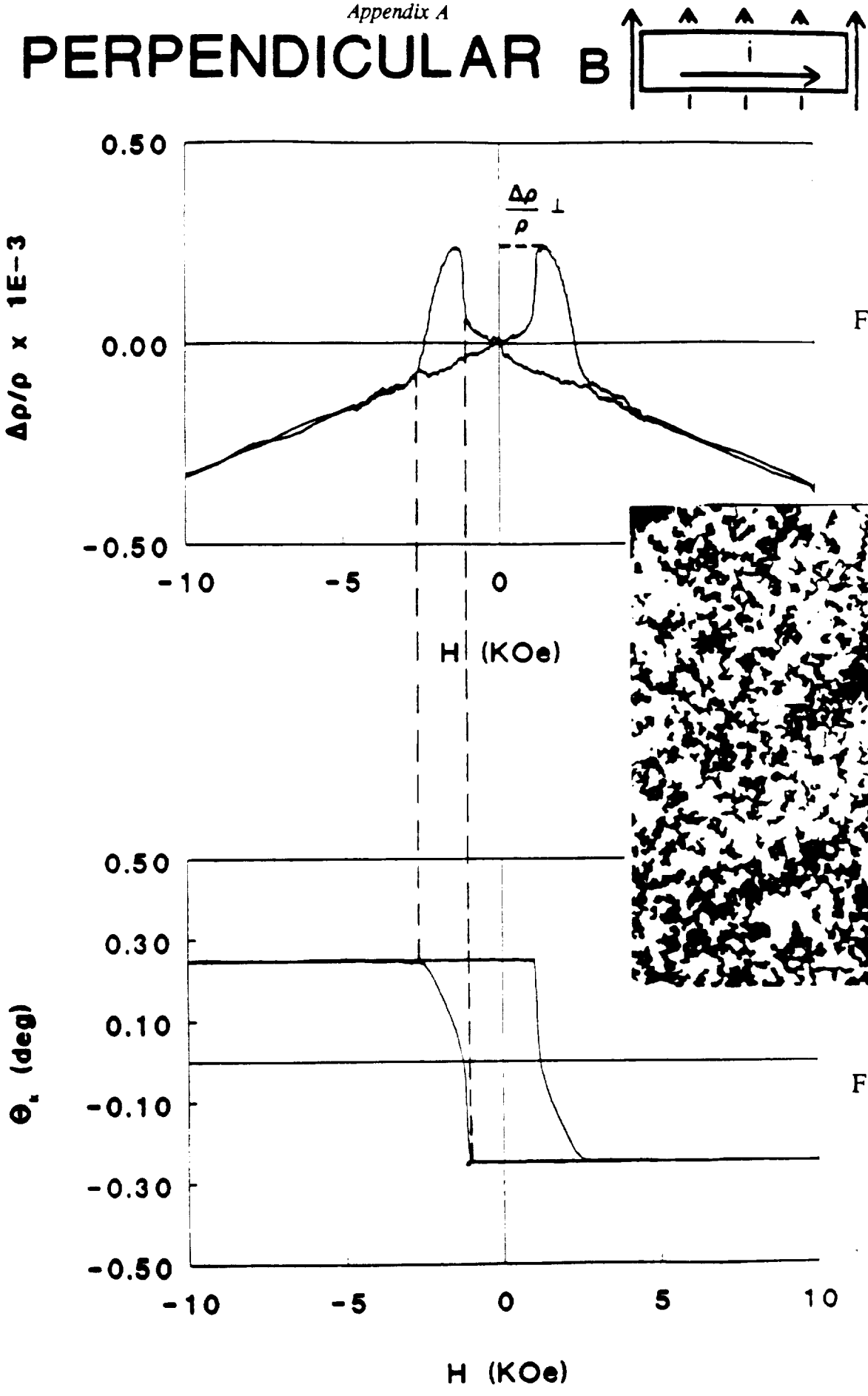

Fig. 7

Fig. 8

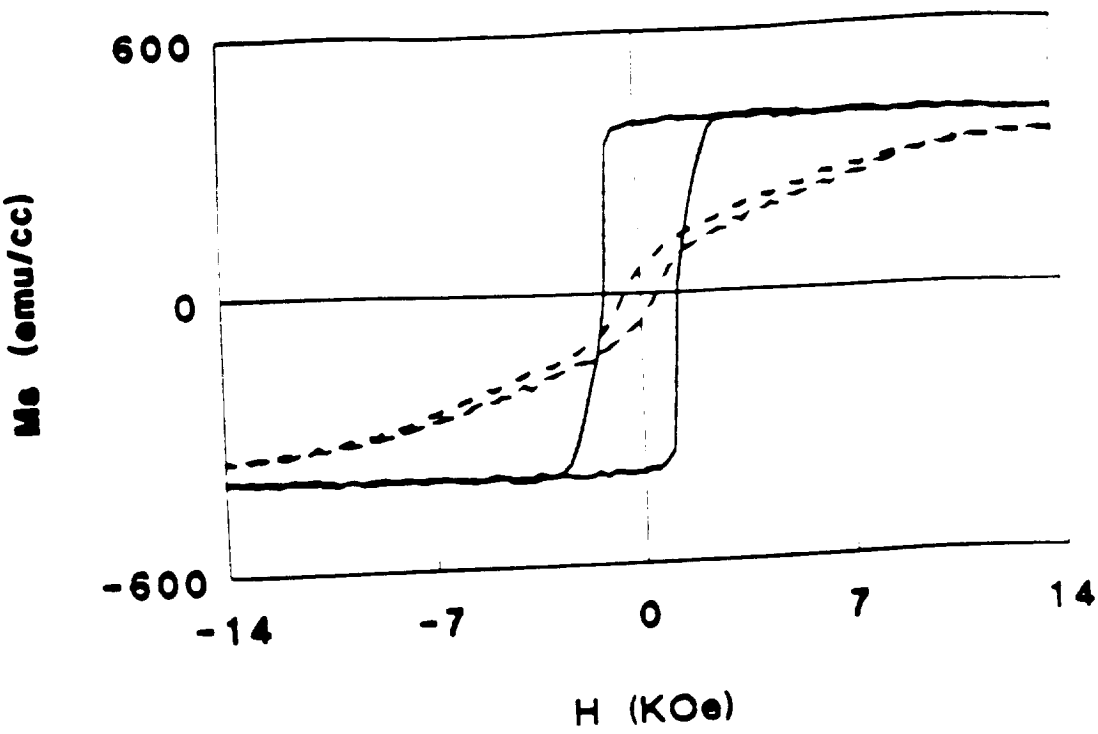

Fig. 9

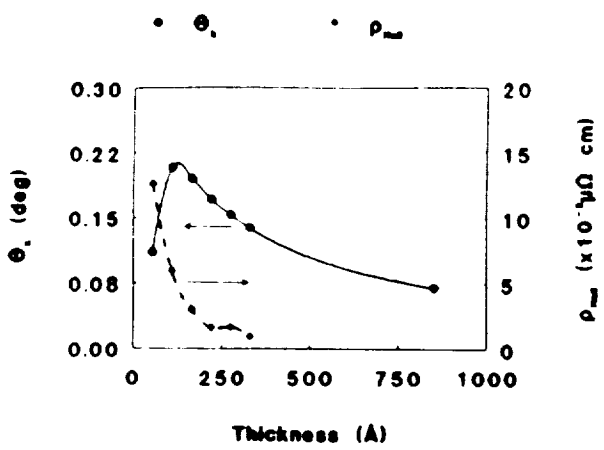

Fig. 10

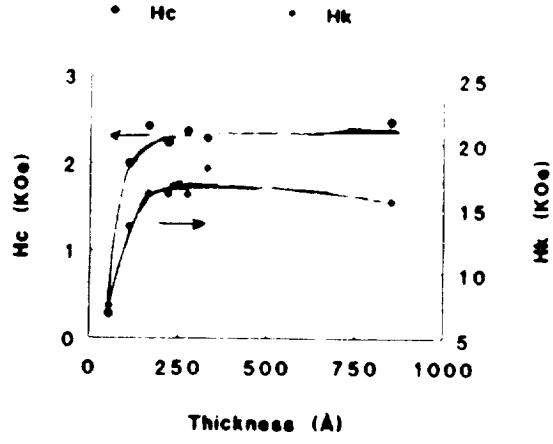

Fig. 11

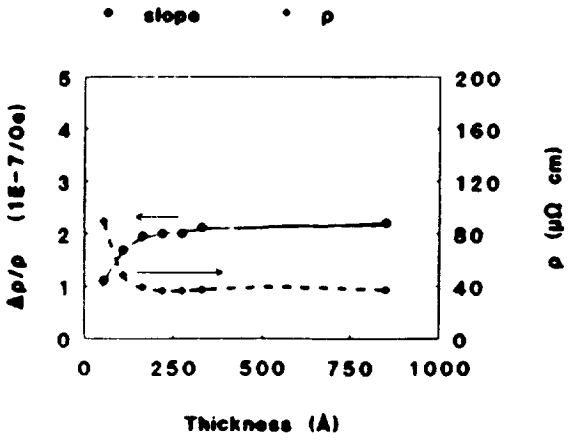

Fig. 12

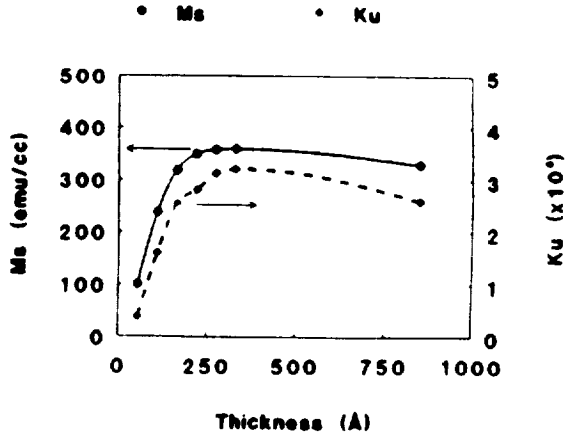

Fig. 13

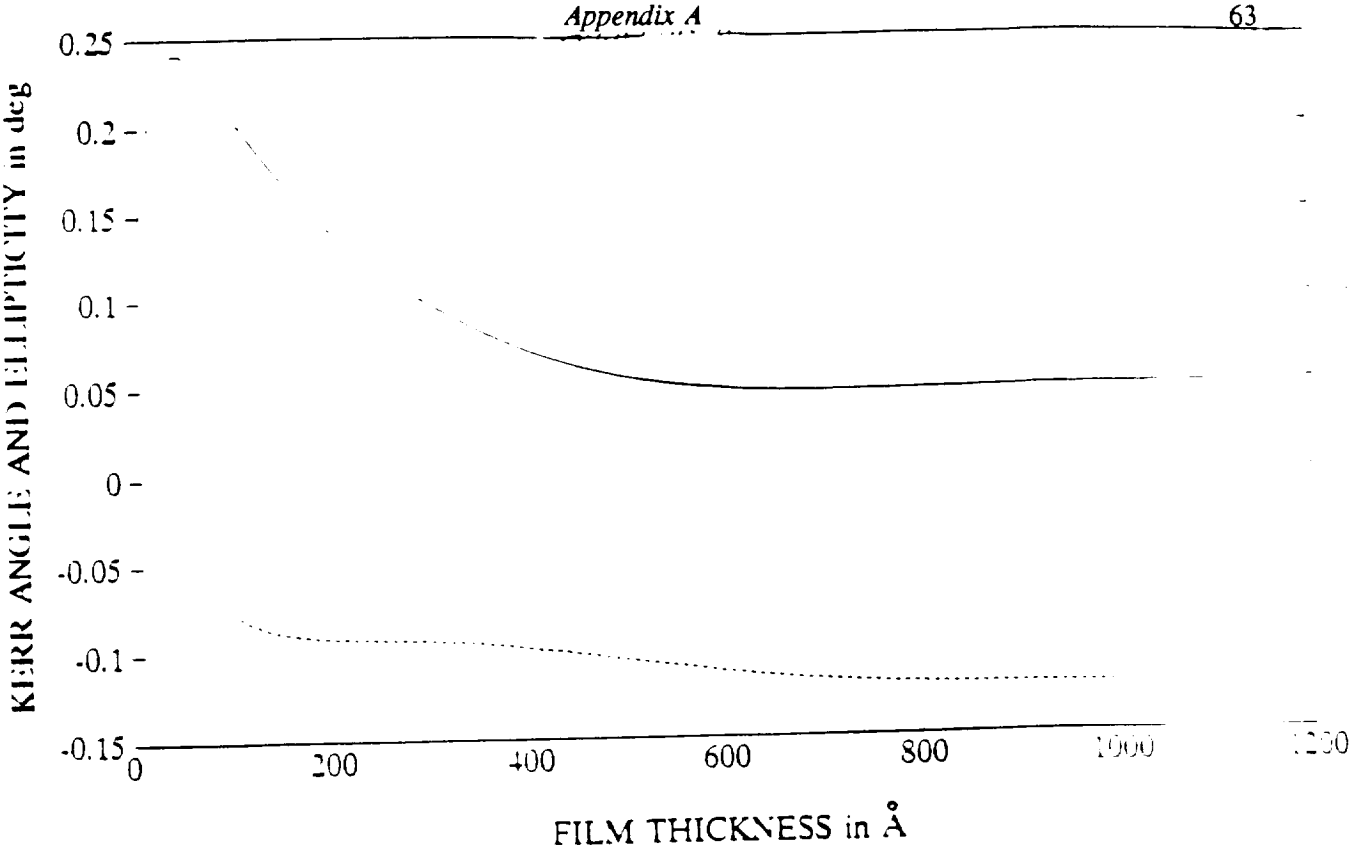

Fig. 14

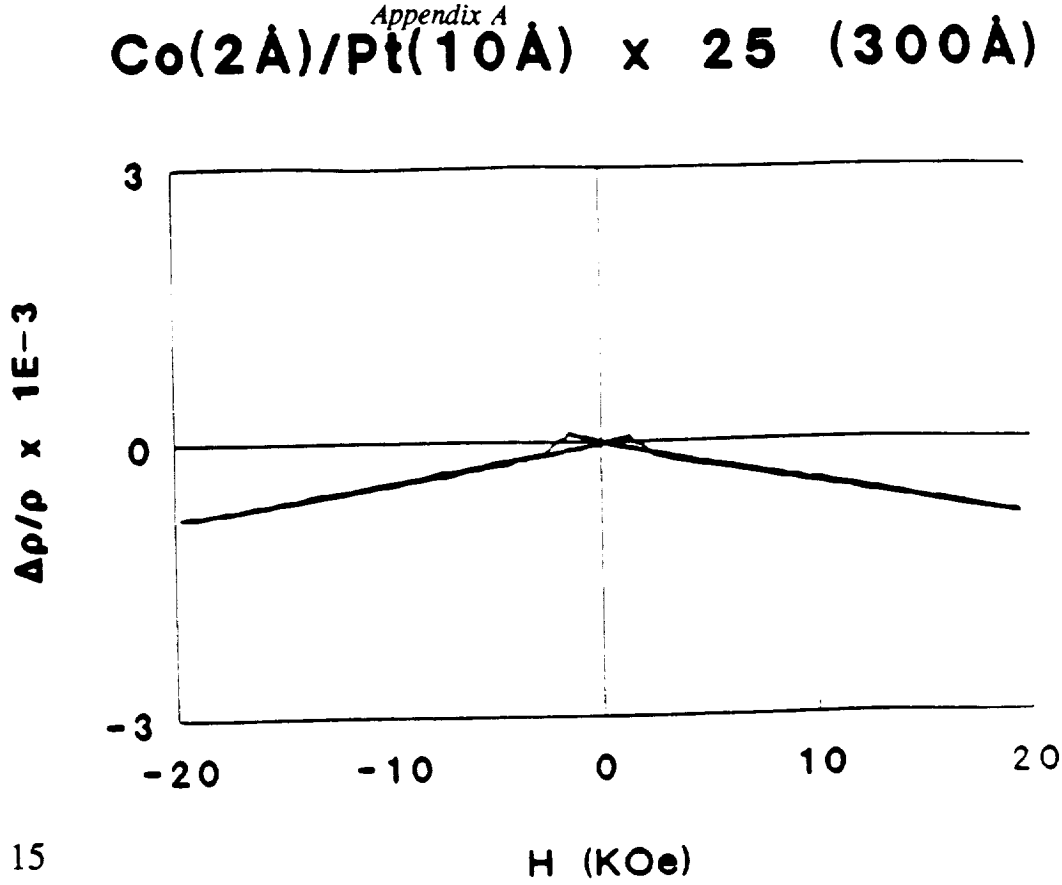
Co(2Å)/Pt(10Å) x 25 (300Å)
3
0
-3
Δρ/ρ x 1E-3
-20
-10
0
10
20
H (KOe)

Fig. 15

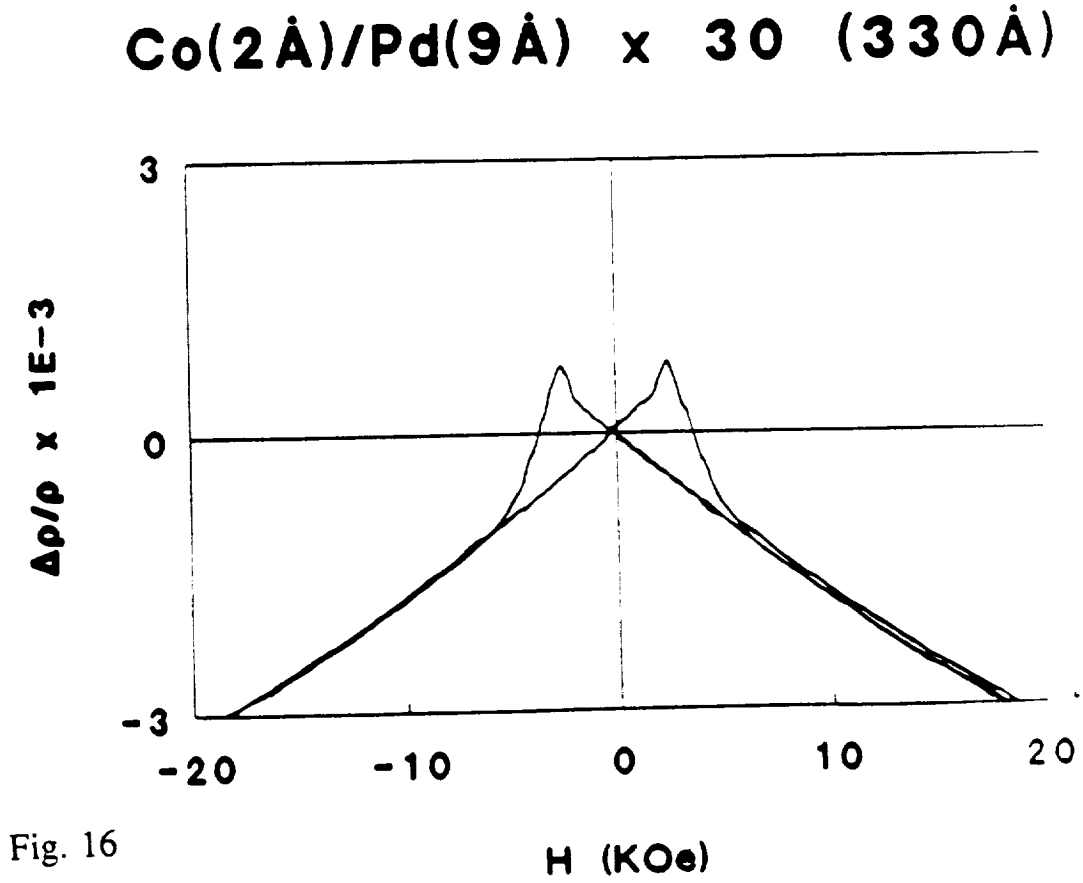
Co(2Å)/Pd(9Å) x 30 (330Å)
3
0
-3
Δρ/ρ x 1E-3
-20
-10
0
10
20
H (KOe)

Fig. 16

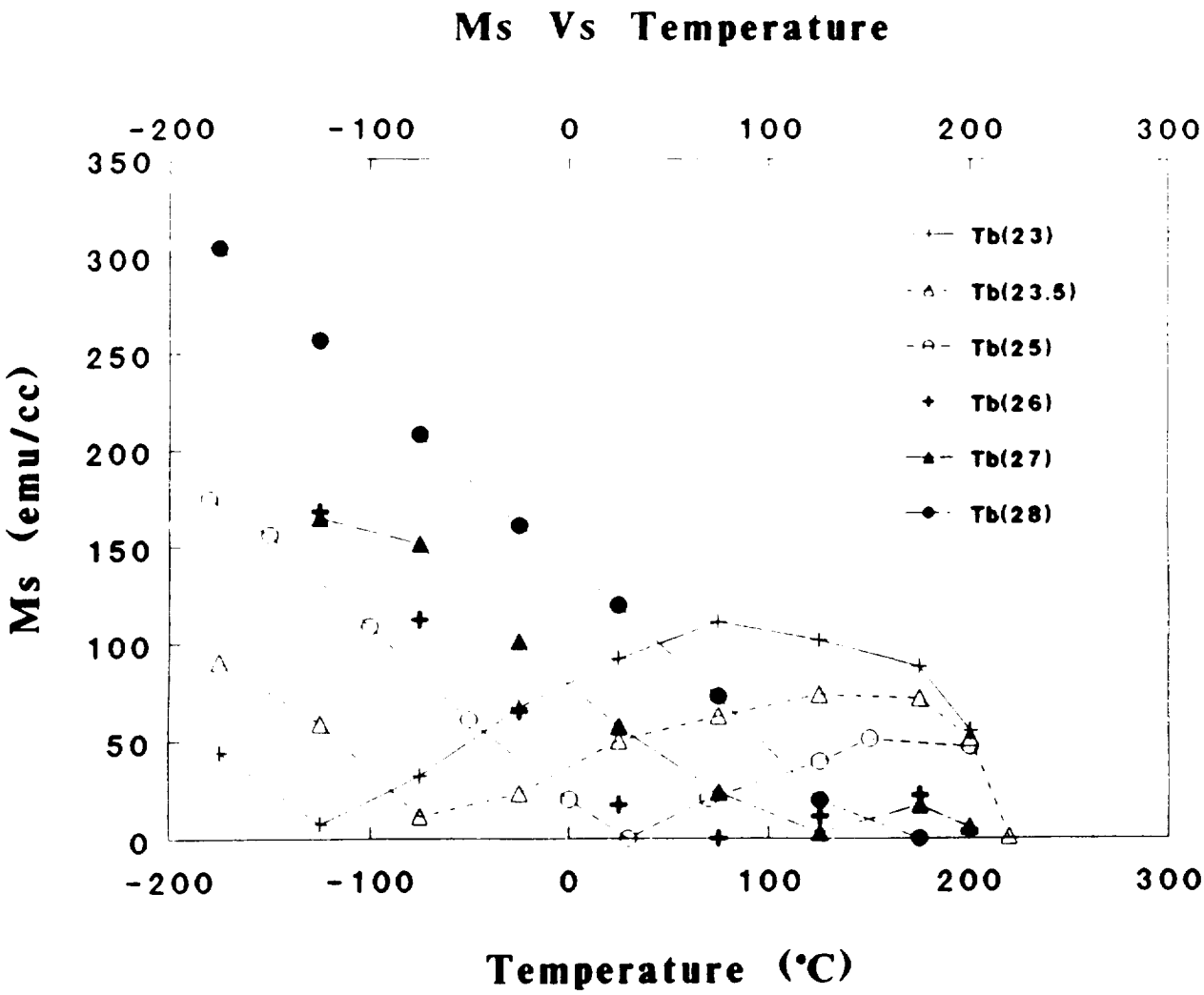
Ms Vs Temperature
-200
-100
0
100
200
300
350
300
250
200
150
100
50
0
Ms (emu/cc)
Tb(23)
Tb(23.5)
Tb(25)
Tb(26)
Tb(27)
Tb(28)
Temperature (°C)

Fig. 17

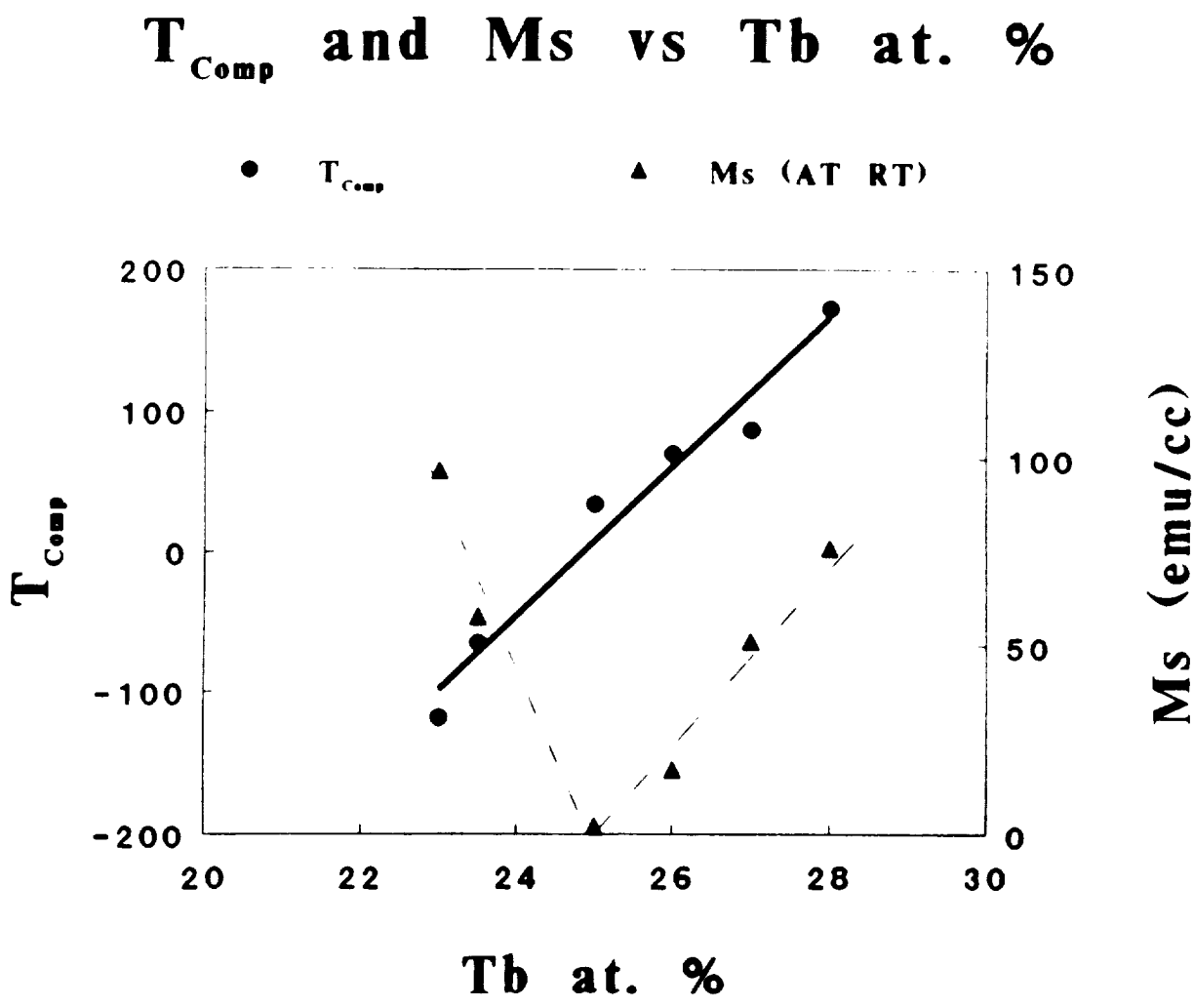
T Comp and Ms vs Tb at. %
T Comp
Ms (AT RT)
200
100
0
-100
-200
150
100
50
0
20
22
24
26
28
30
T Comp
Ms (emu/cc)
Tb at. %

Fig. 18

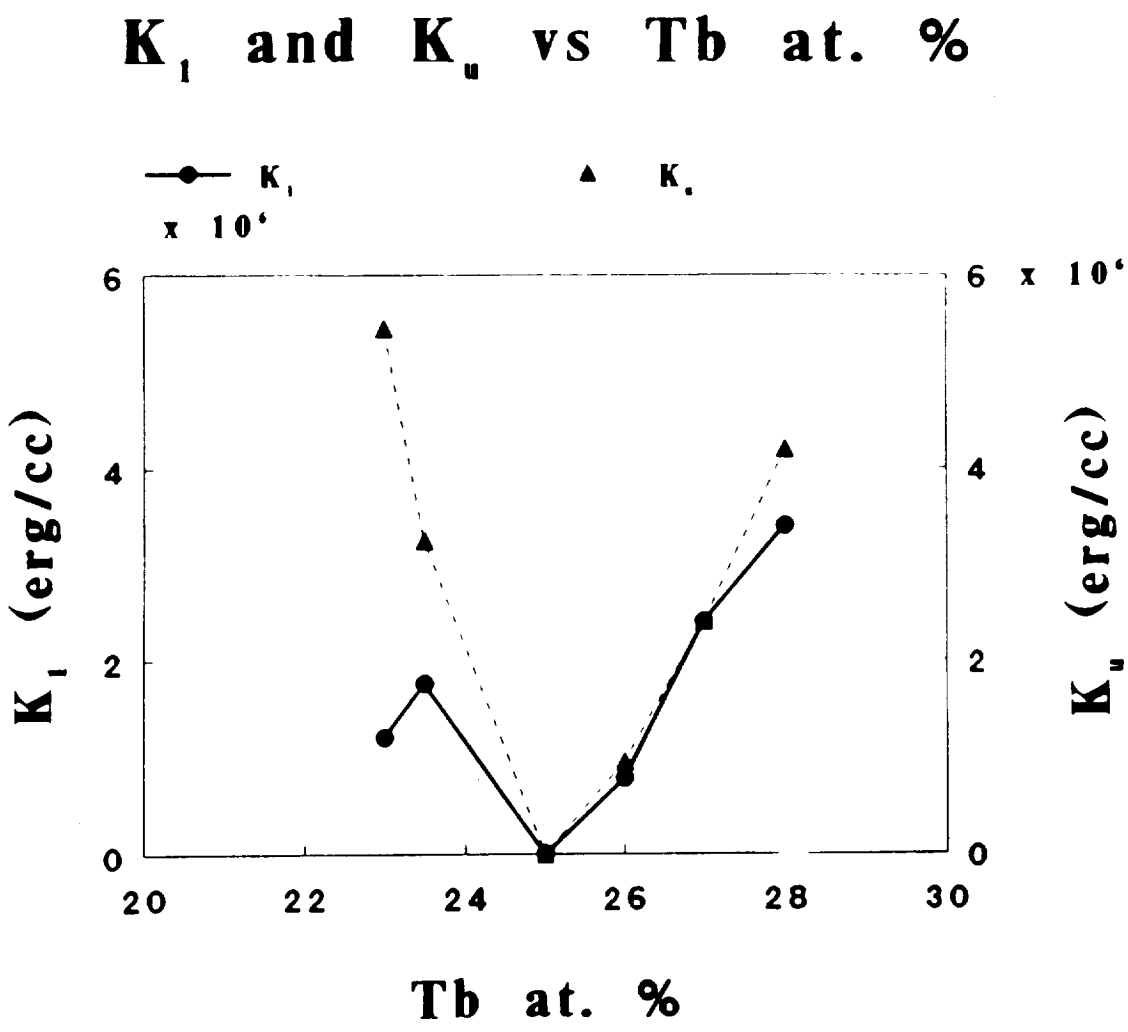
K1 and Ku vs Tb at. %
K1
Ku
x 10⁴
6
4
2
0
20
22
24
26
28
30
K1 (erg/cc)
Ku (erg/cc)
Tb at. %

Fig. 19

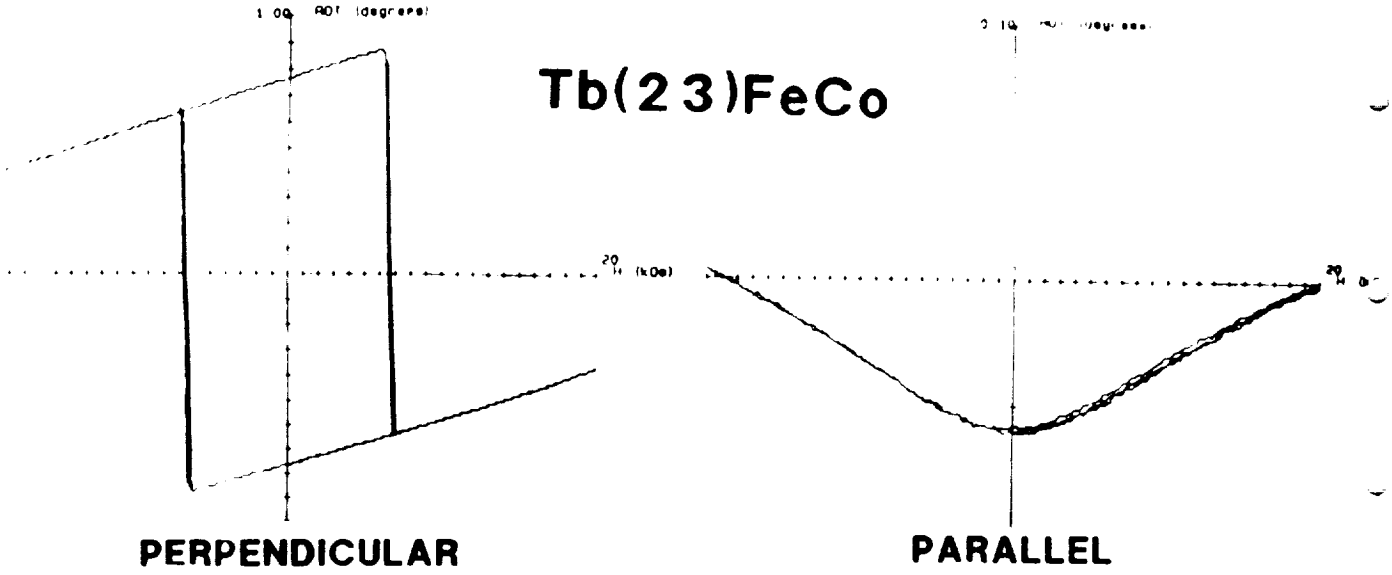

Experimental and theoretical data

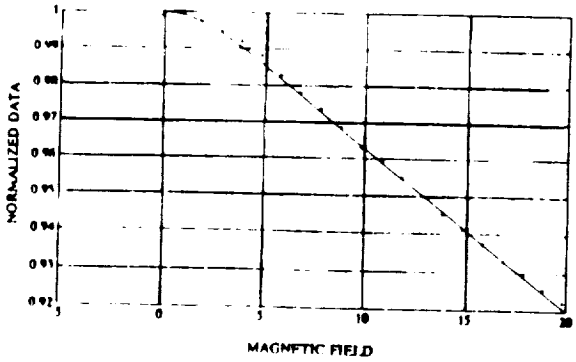

Fig. 20

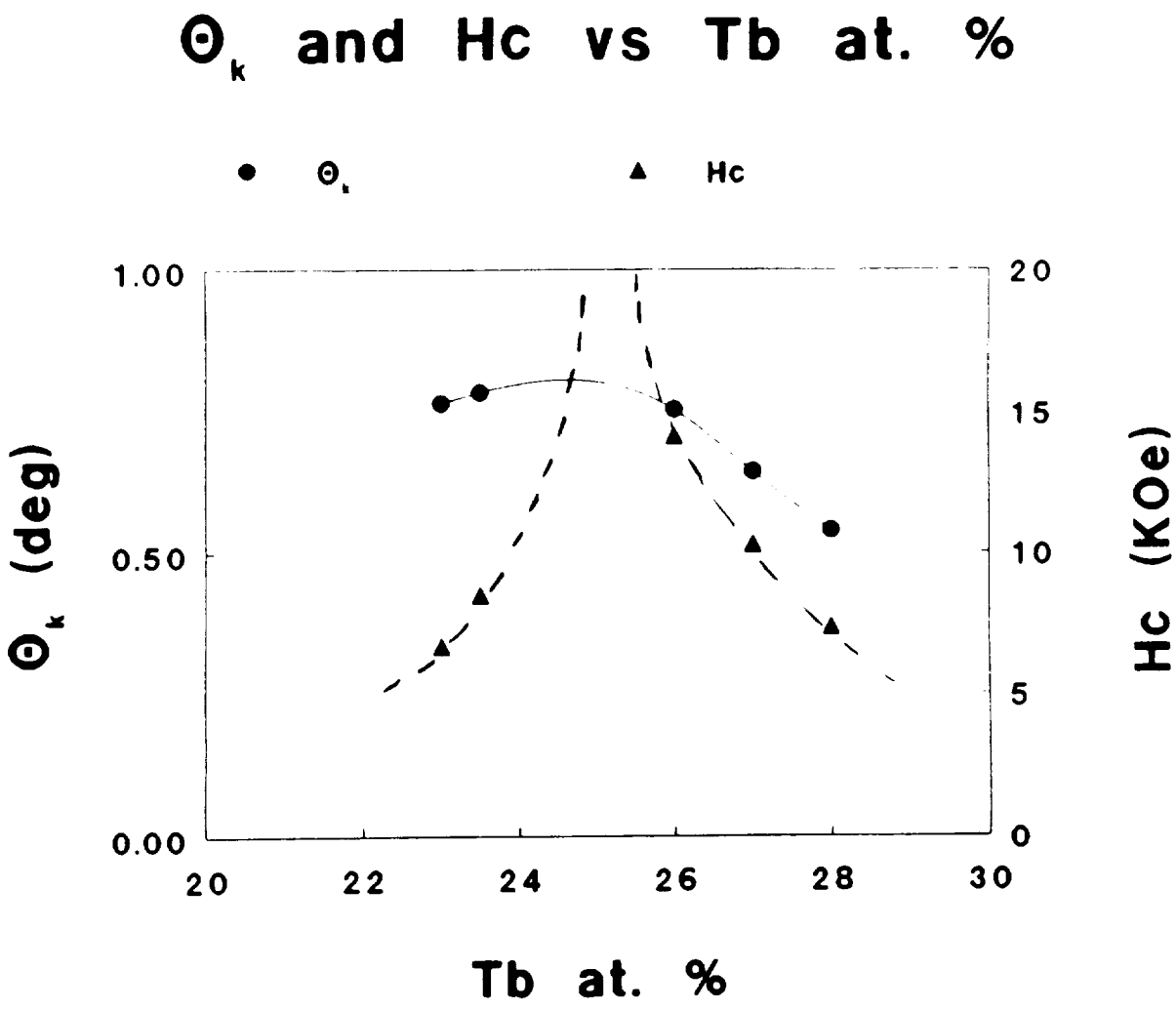
Θk and Hc vs Tb at. %
Θk
Hc
1.00
0.50
0.00
Θk (deg)
20
15
10
5
0
Hc (KOe)
20
22
24
26
28
30
Tb at. %

Fig. 21